

Antiferromagnetic magnetic transition and spin fluctuations in the deformed pyrochlore compound β -Fe₂(OH)₃Cl

M. Fujihala,¹ M. Hagihala,¹ X. G. Zheng,^{1,2,*} and T. Kawae³¹*Department of Physics, Graduate School of Science and Engineering, Saga University, Saga 840-8502, Japan*²*Department of Physics, Faculty of Science and Engineering, Saga University, Saga 840-8502, Japan*³*Department of Applied Quantum Physics and Nuclear Engineering, Faculty of Engineering, Kyushu University, Fukuoka 819-0395, Japan*

(Received 3 April 2010; revised manuscript received 4 July 2010; published 26 July 2010)

Magnetism of the rhombohedral structure Fe₂(OH)₃Cl [β -Fe₂(OH)₃Cl], a member of the geometric frustration series $M_2(\text{OH})_3X$ where the magnetic ions form a deformed pyrochlore lattice, was studied using dc and ac susceptibilities, heat-capacity, neutron powder-diffraction, and muon spin relaxation (μ SR) measurements. Antiferromagnetic transition was observed at $T_N=9.0$ K with a much larger Curie-Weiss temperature θ_w of approximately -64 K, suggesting that Fe₂(OH)₃Cl is a geometrically frustrated magnet. Neutron-diffraction studies revealed the transition into a long-range antiferromagnetic order below $T_N=9.0$ K with the Fe²⁺ spins on the triangular lattice planes disordered, and the other ones on the kagome lattice planes having frozen moments of less than 70% of the full Fe²⁺ moment. Spin fluctuations below T_N were verified further using μ SR studies. The magnetically phase-separated feature and the spin fluctuation coexisting with a long-range magnetic order are considered to be of great interest for studying geometric frustration and the behavior of $S=2$ spin systems on pyrochlore and kagome lattices.

DOI: [10.1103/PhysRevB.82.024425](https://doi.org/10.1103/PhysRevB.82.024425)

PACS number(s): 75.30.-m, 75.25.-j, 75.50.Ee, 76.75.+i

I. INTRODUCTION

Geometrically frustrated magnetic materials show novel magnetic properties because of their lattice geometry.¹ The lattice geometries responsible for frustration are generally triangular lattice, kagome lattice, and pyrochlore lattice. Of particular recent interest are the rare-earth pyrochlore compounds, in which the magnetic ions form networks of corner-shared tetrahedrons and the frustration of spin-spin interactions engenders spin ice states, unconventional spin-glass states, and exotic spin liquid states.²⁻⁹

In recent years, we identified unconventional magnetic transitions in a transition-metal hydroxyhalogenide series of deformed pyrochlore compounds $M_2(\text{OH})_3X$, where M represents a d -electron magnetic ion such as Cu²⁺, Ni²⁺, Co²⁺, Fe²⁺, and Mn²⁺ and X represents the halogen ions of Cl⁻¹, Br⁻¹, or I⁻¹.¹⁰⁻¹⁴ Much of these metal hydroxyhalogenides were found originally in natural minerals. This material category presents a complete series for spins $S=1/2$ to $S=5/2$ ($S=1/2$ for Cu²⁺, 1 for Ni²⁺, 3/2 for Co²⁺, 2 for Fe²⁺, and 5/2 for Mn²⁺). In particular, clinoatacamite, Cu₂(OH)₃Cl, transitions at $T_{N1}=18.1$ K with a very small entropy release, $T_{N2}=6.4$ K and $T_{N3}=6.2$ K with coexisting order and spin fluctuation. The nature of the $T_{N1}=18.1$ K phase remains largely unknown and attracts much interest.¹⁵⁻¹⁷ Furthermore, it is the first example of the $S=1/2$ Heisenberg quantum spin on a pyrochlore lattice and the parent compound for the substituted “perfect kagome lattice” of herbertsmithite ZnCu₃Cl₂(OH)₆, which exhibits spin liquid behavior.^{18,19}

Fe₂(OH)₃Cl is the $S=2$ spin system of the transition-metal hydroxyhalogenide series. As exemplified in the Cu²⁺ series of atacamite, clinoatacamite, and botallackite,¹¹ the transition-metal hydroxyhalogenide series usually have multiple polymorphous structures. Three crystal structures of Fe₂(OH)₃Cl have been reported: the hexagonal

α -Fe₂(OH)₃Cl, the rhombohedral β -Fe₂(OH)₃Cl,^{20,21} and the orthorhombic γ -Fe₂(OH)₃Cl (Hibbingite).²² As shown in the present work, the Fe²⁺ ions in β -Fe₂(OH)₃Cl form a deformed pyrochlore lattice like the rhombohedral Co₂(OH)₃Cl, in which we observed geometric frustration.¹² Only a few works in the fields of mineralogy, meteorology, and corrosion science have examined Fe₂(OH)₃Cl compounds. The present work reports the magnetism and the detailed structure information of the deformed pyrochlore lattice β -Fe₂(OH)₃Cl.

II. EXPERIMENTAL PROCEDURES

White powders of polycrystalline samples of β -Fe₂(OH)₃Cl [Fe₂(OD)₃Cl for neutron diffraction] were prepared using a hydrothermal reaction of aqueous solutions of 3.5M FeCl₂ 6H₂O [dried FeCl₂ for Fe₂(OD)₃Cl] and 5M NaOH [NaOD for Fe₂(OD)₃Cl] at around 80 °C for several hours in a nitrogen-gas atmosphere. Exposure to air was avoided because β -Fe₂(OH)₃Cl would thereby be oxidized, changing color quickly to brownish in air. The crystal structure was investigated using synchrotron x-ray diffraction at the BL02B2 beam line at the SPring-8 synchrotron using a Debye-Scherrer camera with an imaging plate.²³ The incident x-ray beam was monochromatized using a double-crystal monochromator tuned to the wavelength of approximately 0.5 Å (precisely determined using standard sample of CeO₂ to be 0.50217 Å). Powder-diffraction patterns were collected over the 2θ range of 3°–75° in a step angle of 0.01°. The unit-cell parameters were first calculated roughly from observed d value and hkl peak data of the powder-diffraction data using a least-squares method. Then they were refined using the Rietveld method with a computer program RIETAN-2000.²⁴ The dc and ac susceptibilities measurements were taken using a commercial superconducting quantum in-

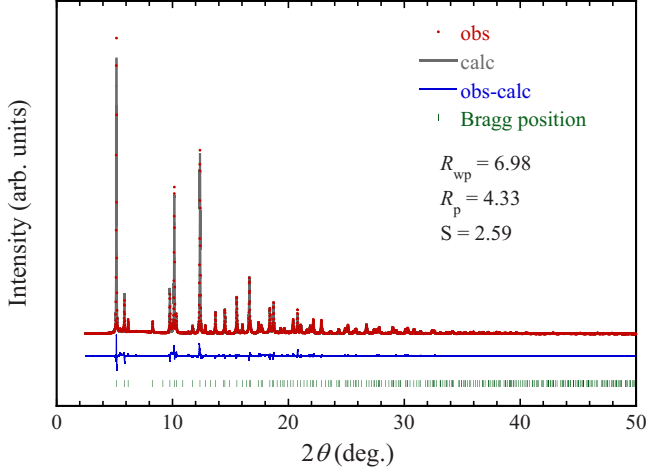


FIG. 1. (Color online) Synchrotron x-ray diffraction pattern (filled circles) for $\text{Fe}_2(\text{OH})_3\text{Cl}$ at 300 K and the result of Rietveld structure refinements showing the calculated (thick solid line) pattern and the difference (thin solid line below the XRD spectra).

terference device magnetometer (MPMS; Quantum Design). The heat capacity was measured using an adiabatic heat-pulse method with a ^3He cryostat using an amount of 0.4 g of the polycrystalline powder. A neutron powder-diffraction experiment was performed with a wavelength of 1.8264 Å using a Kinken powder diffractometer, HERMES, of the Institute for Materials Research (IMR), Tohoku University, installed at the JRR-3M reactor at the Japan Atomic Energy Research Institute (JAERI), Tokai.²⁵ The collected neutron data were refined using the program FULLPROF suite based on Rietveld refinement.²² Muon spin rotation/relaxation (μSR) experiments were conducted on M20 port at TRIUMF

(Canada) using a positive surface muon beam with a conventional He-gas flow cryostat. The positive muon beam, polarized to the beam direction, is stopped in the specimen and depolarized by its internal field. The time histograms of muon decay positrons are recorded by forward (F) and backward (B) counters as a function of resident time for each μ^+ within the specimen. A positron is emitted preferentially toward the muon spin direction. Therefore, asymmetry $a(t) = [F(t) - B(t)] / [F(t) + B(t)]$ of the two histograms (after correction for solid-angle effects) reflects the time evolution of muon spin polarization, as well as the time evolution and space distribution of the internal field in the specimen.

III. RESULTS AND DISCUSSION

A. Structure characterization and magnetic properties

The rhombohedral $\text{Fe}_2(\text{OH})_3\text{Cl}$ was synthesized in single phase, as demonstrated by the synchrotron x-ray diffraction pattern and the Rietveld fit presented in Fig. 1. Consistent with Ref. 20, it is a rhombohedral structure in the space group $R\bar{3}m$, the lattice parameters was refined to be $a = 6.94139(8)$ Å and $c = 14.72709(21)$ Å. The positions of the individual atoms were also determined as presented in Table I. For determination of the hydrogen atoms neutron powder-diffraction data on $\text{Fe}_2(\text{OD})_3\text{Cl}$ at 12 K was analyzed similarly using the Rietveld fit. The results are presented in Table II. The magnetic ions of Fe^{2+} in $\beta\text{-Fe}_2(\text{OH})_3\text{Cl}$ form a three-dimensional network of linked tetrahedrons that can be viewed as alternative stacking layers of kagome and triangular lattice planes in the (001) direction (Fig. 2). A prominent structural feature is a notable distortion in the tetrahedron where the $\text{Fe}^{2+}\text{-Fe}^{2+}$ distance on the kagome lattice planes

TABLE I. Structure information of synthetic $\beta\text{-Fe}_2(\text{OH})_3\text{Cl}$ refined from synchrotron x-ray diffraction data obtained at 300 K.

Chemical formula		$\text{Fe}_2(\text{OH})_3\text{Cl}$					
Cell setting		Rhombohedral					
Space group		$R\bar{3}m$ (no. 166)					
a (Å)		6.94139(8)					
c (Å)		14.72709(21)					
V (Å ³)		614.526 (13)					
$R_{\text{wp}}(S)$		6.98 (2.59)					
R_{p}		4.33					
	x	y	z	g	B	Site	Sym.
Fe1	0.50000	0.00000	0.00000	1.000	0.807(16)	9e	2/m
Fe2	0.00000	0.00000	0.50000	1.000	0.807(16)	3b	$\bar{3}m$
Cl	0.00000	0.00000	0.21620(13)	1.000	0.950(33)	6c	3m
O	0.19899(17)	0.39799	0.07180(13)	1.000	0.968(66)	18h	m
				Bond length (Å)			
$\text{Fe}_K\text{-Fe}_K$				3.47069			
$\text{Fe}_T\text{-Fe}_K$				3.16858			

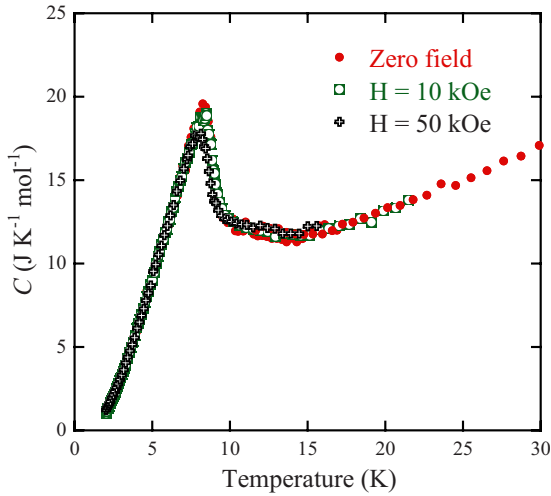


FIG. 4. (Color online) Temperature dependence of total specific heat $C(T)$ per mole of $\text{Fe}_2(\text{OH})_3\text{Cl}$ under a zero field, 10 kOe, and 50 kOe, respectively. The small upturn at around 14 K was caused by the inclusion of a polymorphous phase of $\text{Fe}_2(\text{OH})_3\text{Cl}$, which undergoes an antiferromagnetic transition at $T_N=14$ K as we previously reported in Ref. 13. It is hard to subtract the lattice contribution from the specific heat, therefore, the magnetic entropy is not estimated.

magnetic field induced a ferromagnetic state. The stability of the antiferromagnetism in $\text{Fe}_2(\text{OH})_3\text{Cl}$ is considered to be related to its magnetic spin structure, as is discussed below.

B. Possible magnetic structures from neutron diffraction

Neutron-diffraction patterns obtained with the powder sample of $\text{Fe}_2(\text{OD})_3\text{Cl}$ at 12 K and 3.5 K, respectively, are depicted in Fig. 5. Long-range antiferromagnetic order developed below the transition temperature. The magnetic reflections can be indexed by $k=(0\ 0\ 3/2)$, as marked in Fig. 5. Consistent with the susceptibility measurements, a broad

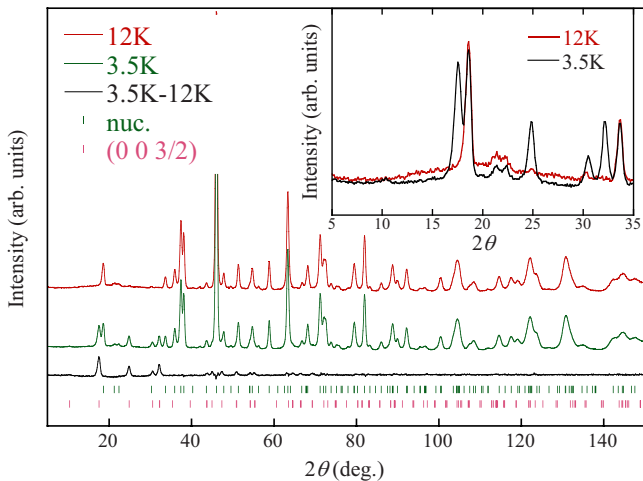


FIG. 5. (Color online) Neutron-diffraction patterns obtained, respectively, for $\text{Fe}_2(\text{OD})_3\text{Cl}$ at 12 and 3.5 K. The difference between 12 and 3.5 K is presented on the bottom depicting the magnetic reflection peaks. The inset is an enlarged plot for the low-angle part.

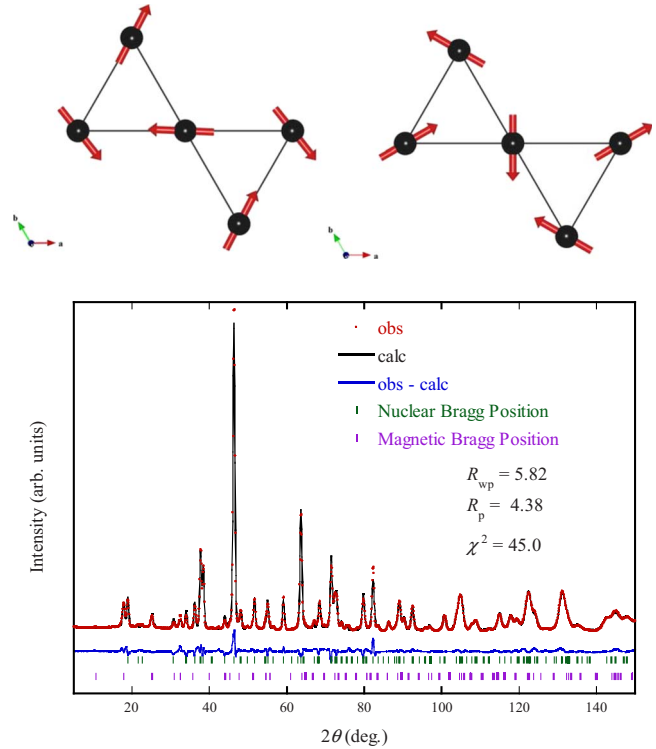


FIG. 6. (Color online) [(a) and (b)] Proposed magnetic structures with spin order only occurring on the kagome lattice planes. (c) The calculated neutron-diffraction pattern using either of the magnetic structures for $\text{Fe}_2(\text{OD})_3\text{Cl}$.

peak (the inset plot) is apparent at 12 K and higher temperatures, suggesting a short-range spin correlation well above the T_N .

Possible magnetic structures were explored using a representation analysis technique.²⁶ The intensities of the magnetic reflection peaks are relatively low as compared with the full moment of Fe^{2+} . Good fit was obtained by assuming the spin structures illustrated in Figs. 6(a) and 6(b), respectively, in which the Fe^{2+} spin order occurs on the kagome lattice planes but with the spin directions aligned differently. Equivalent goodness of fitting was obtained for the two spin configurations, therefore, further determination only can be made with a single-crystal experiment. The results of the Rietveld refinement of the 3.5 K diffraction pattern for one of them are shown in Fig. 6(c). Another type of candidate structures is shown in Figs. 7(a) and 7(b). The Fe^{2+} on the triangular lattice planes also shows a frozen moment while the Fe^{2+} ions on the kagome lattice planes keep any of the two configurations shown in Figs. 6(a) and 6(b). The Rietveld refinement results are shown in Fig. 7(c). For the two models portrayed in Figs. 6(a) and 6(b) only the three Fe^{2+} ions on the kagome lattice plane are ordered with two of them having magnetic moments of $3.70\mu_B$ and the third one $3.36\mu_B$. For the models presented in Figs. 7(a) and 7(b) the Fe^{2+} ion on the triangular lattice plane has a small ordered moment of $1.05\mu_B$, and the two Fe^{2+} ions on the kagome lattice plane have moments of $3.57\mu_B$ and the third one $3.62\mu_B$. As a matter of fact, the two models in Figs. 7(a) and 7(b) can be viewed as slightly modified version of those

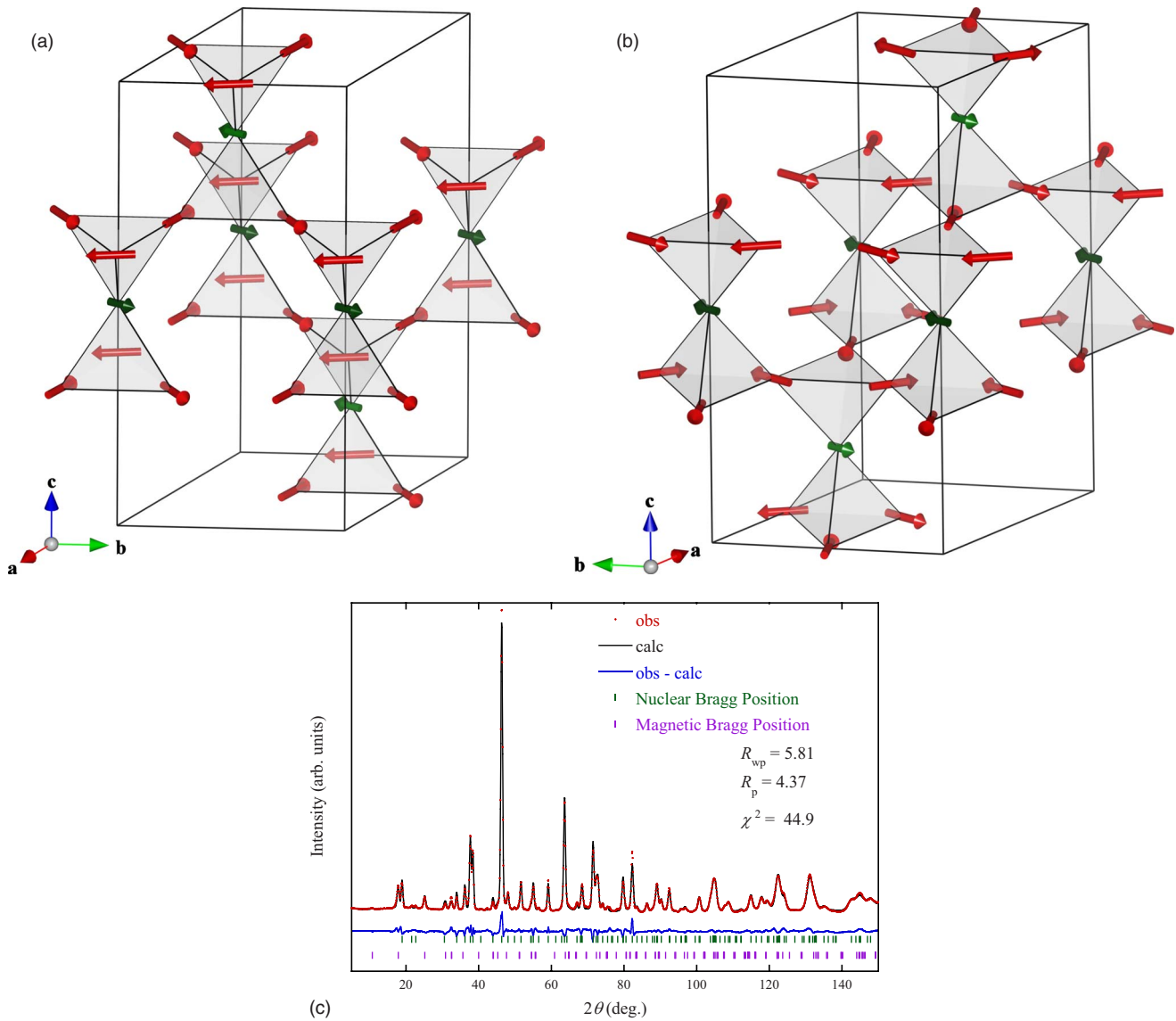


FIG. 7. (Color online) [(a) and (b)] Proposed magnetic structures with spin order occurring both on the kagome lattice planes as well as the triangular lattice planes. (c) The calculated neutron-diffraction pattern using the proposed magnetic structures for $\text{Fe}_2(\text{OD})_3\text{Cl}$.

shown in Figs. 6(a) and 6(b), the moment on the triangular lattice plane compensated for the decreased moments on the kagome lattice plane. As the refinement plots show, it is difficult to determine which one is the correct magnetic structure from the powder-diffraction data. Nevertheless, in all models, the ordered magnetic moments are mostly residing on the kagome lattice planes. Furthermore, they are remarkably smaller than the full moment of Fe^{2+} ($5.3\mu_B$, as estimated from the magnetic susceptibilities). This fact suggests almost disordered Fe^{2+} on the triangular lattice planes, as well as remaining spin fluctuation for the ordered Fe^{2+} on the kagome lattice planes. The image of weakly coupled kagome lattice planes is drastically different from that of $\text{Co}_2(\text{OH})_3\text{Cl}$ (Ref. 12) and $\text{Co}_2(\text{OH})_3\text{Br}$ which share the same crystal structure as $\text{Fe}_2(\text{OH})_3\text{Cl}$. In $\text{Co}_2(\text{OH})_3\text{Cl}$ the spins on the triangular lattice planes are ferromagnetically ordered while in antiferromagnetic $\text{Co}_2(\text{OH})_3\text{Br}$ external magnetic field induced transitions into ferromagnetic states. The stability of the antiferromagnetic state in $\text{Fe}_2(\text{OH})_3\text{Cl}$, as shown by the

specific heat in Fig. 4, may be related to its Heisenberg-type two-dimensional magnetic structure.

The reason why the Fe^{2+} spins on the triangular lattice planes have stronger fluctuation than those on the kagome lattice planes can be found in its lattice structure. As seen in Fig. 2, the three Fe^{2+} ions (denoted by Fe_K) on the kagome lattice planes are in a highly symmetric position surrounded by nearby O^- and Cl^- ions but the Fe^{2+} ion (denoted by Fe_T) on the triangular lattice plane is only surrounded by O^- . The distance of the Fe_K -O bonding is 2.123 Å and the bonding angle of Fe_K -O- Fe_K is 109.7° while the Fe_T -O bonding has a longer distance of 2.135 Å and a smaller angle of 96.17° for Fe_T -O- Fe_K . If we assume superexchange interactions for the antiferromagnetism through the Fe-O-Fe bonding, apparently one can expect stronger coupling for the Fe_K ions on the kagome lattice planes. Moreover, from our previous studies on the hydroxyhalogenide series we learned that larger halogen ions effectively enhanced the superexchange coupling. For example, in botallackite-structure $\text{Cu}_2(\text{OH})_3\text{X}$ (X

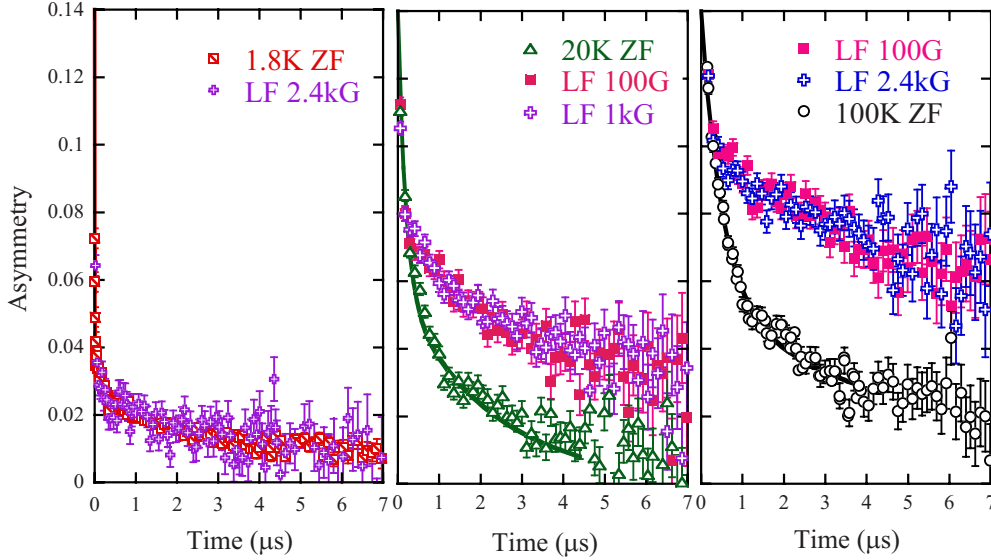


FIG. 8. (Color online) LF- μ SR asymmetries for polycrystalline $\text{Fe}_2(\text{OH})_3\text{Cl}$ at 100 K, 20 K, and 1.8 K, respectively.

=Cl,Br,I) [although their crystal structure is different from the present $\text{Fe}_2(\text{OH})_3\text{Cl}$, the Cu-X bonding has a similar coordination as the Fe-Cl in $\text{Fe}_2(\text{OH})_3\text{Cl}$], the T_N increased from $T_N=7.2$ K for $\text{Cu}_2(\text{OH})_3\text{Cl}$ to $T_N=10$ K for $\text{Cu}_2(\text{OH})_3\text{Br}$ and $T_N=14$ K for $\text{Cu}_2(\text{OH})_3\text{I}$, respectively.¹⁴ The enhanced antiferromagnetic coupling by larger halogen ions was also demonstrated in the case of pyrochlore $\text{Co}_2(\text{OH})_3\text{Cl}$ and $\text{Co}_2(\text{OH})_3\text{Br}$, which show the same crystal structure as the present $\text{Fe}_2(\text{OH})_3\text{Cl}$. Replacing Cl with Br leads to transformation from a partial ferromagnetic order in $\text{Co}_2(\text{OH})_3\text{Cl}$ into an antiferromagnetic order in $\text{Co}_2(\text{OH})_3\text{Br}$ [Ref. 13 and unpublished data]. All of the above-mentioned results suggest strong superexchange interactions through the halogen ions. Therefore, we can safely conclude that strong coupling through the $\text{Fe}_K\text{-Cl-Fe}_K$ bonding dominates in the present material $\text{Fe}_2(\text{OH})_3\text{Cl}$.

C. Investigation of spin dynamics with μ SR

As many μ SR studies have demonstrated, in addition to being a direct probe showing magnetic order, the positive muon μ^+ is a sensitive probe to investigate spin fluctuation in the frustrated magnetic materials.^{6,12,18,27-30} In the magnetically ordered state of a polycrystalline sample, the longitudinal polarization function $P_Z(t)$ is expected to be the weighted sum of longitudinal and transverse components: $P_Z(t) = [\exp(-\lambda_Z t) + 2 \exp(-\lambda_X t) \cos(\gamma_\mu \langle B_{\text{loc}} \rangle t)] / 3$. Therein, λ_Z and λ_X , respectively, denote the spin-lattice and spin-spin relaxation rates, γ_μ is the muon gyromagnetic ratio ($\gamma_\mu = 2\pi \times 135.5$ MHz/T), and $\langle B_{\text{loc}} \rangle$ stands for the mean value of the local field at the muon site.

Therefore, we further studied the spin dynamics using zero-field (ZF) and longitudinal field (LF) muon spin relaxation (μ SR) measurements. In $\text{Fe}_2(\text{OH})_3\text{Cl}$, four possible stopping sites exist for the positive muons: one near the Cl and three near the three O ions. The positive muons feel the local fields produced by the nuclei moments and the electron spins of Fe^{2+} . In a paramagnetic state, when the magnetic

coupling of the electron spins is not present, the field of the electron spins is fluctuating too fast to be detected by the muons. Therefore, the muons only detect those nuclei fields which look static to the muons. The muon spin depolarization is expressed using a static Kubo-Toyabe function. It is decoupled in a weak external field. Some typical ZF and LF μ SR asymmetries at representative temperatures are presented in Fig. 8. Even at 100 K, muon spin depolarization was observed, which remained in a strong magnetic field of 2400 G, suggesting the existence of dynamic field, i.e., the existence of $\text{Fe}^{2+}\text{-Fe}^{2+}$ spin coupling, at high temperatures. The decoupled proportion decreased to approximately 20% at 20 K (Fig. 8), which is attributed to the muons on the Cl site distant from the Fe^{2+} spins (refer to the crystal structure in Fig. 2).

The ZF- μ SR asymmetries at typical temperatures are presented in Fig. 9. The depolarization accelerates quickly below around 30 K. The ZF- μ SR asymmetry for $T > T_N$ are

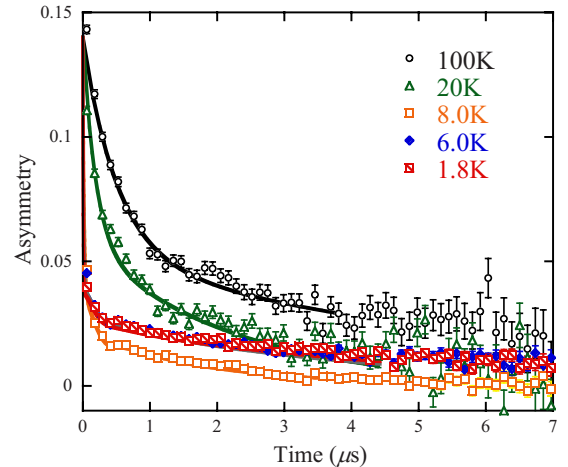


FIG. 9. (Color online) ZF- μ SR asymmetries for polycrystalline $\text{Fe}_2(\text{OH})_3\text{Cl}$ at typical temperatures. The solid lines are calculated to fit as described in the text.

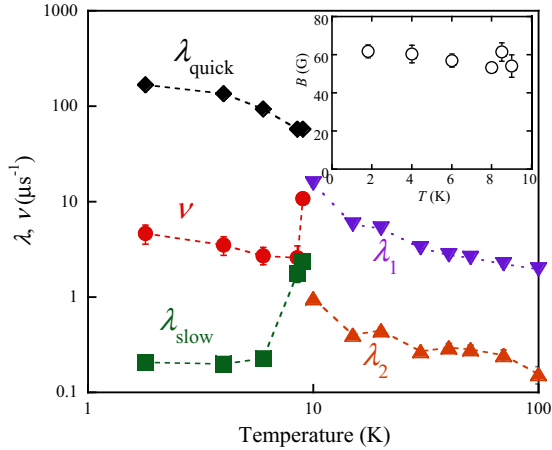


FIG. 10. (Color online) Temperature dependences of the fitted parameters. The inset plot shows the estimated local fields in the dynamic Kubo-Toyabe function.

best fit by two exponential functions, $a_0 P_Z(t) = a_1 \exp(-\lambda_1 t) + a_2 \exp(-\lambda_2 t)$, wherein the two depolarization rates differ remarkably, as presented in Fig. 10. When the temperature approaches $T_N = 9$ K, both depolarization rates increased rapidly, implying a critical slowing toward T_N .

For $T < T_N$, the best fit was obtained with the sum of two exponential functions and a dynamic Kubo-Toyabe function as

$$a_0 P_Z(t) = \exp(-\lambda_q t) + a_s \exp(-\lambda_s t) + a_D G^{\text{DGKT}}(t, \Delta, \nu),$$

where λ_q denotes a quick depolarization and λ_s a slow one. Here, $G^{\text{DGKT}}(t, \Delta, \nu)$ is the dynamic Kubo-Toyabe relaxation function, where Δ is a measure of the local field by $\Delta = \sqrt{B_{\text{loc}}^2}$, ν is a reciprocal of τ_c , which is the interval of time during which the muons detect the change in the local magnetic field.³¹ When Δ/ν is approximately 1, $G^{\text{DGKT}}(t, \Delta, \nu)$ is approximately expressed by the exponential function of $\exp(-\Delta^2 t/\nu)$. A small Δ of approximately 50 G was estimated as shown in the inset plot in Fig. 10. Based on the depolarization proportion as well as the small Δ , we presume that the dynamic Kubo-Toyabe function represents the muon spin depolarization on the Cl sites. The other two exponential functions therefore reflect the strong local fields near the O sites immediately outside of the Fe^{2+} tetrahedron.

It is worth noting that although the long-range magnetic order is clearly demonstrated, no oscillations responding to it were observed, which differs from $\text{Co}_2(\text{OH})_3\text{Cl}$, for which oscillations of 50 MHz were observed.¹² Instead, the μSR data suggest spin fluctuation on different time scales. The oscillation signals might be absent because they are wiped by the dynamical fields or the magnetic order is a novel “dynamical long-range order,” as proposed for the “ordered spin ice:” $\text{Tb}_2\text{Sn}_2\text{O}_7$.^{29,30} The μSR result is consistent with the proposed models for the magnetic structure by the neutron-diffraction study, which suggests a remaining spin fluctuation of drastically different spins (spins with zero or a small mo-

ment of $1.05\mu_B$ on the triangular lattice planes, and spins with $3.36\mu_B - 3.70\mu_B$ on kagome lattice planes). Apparently, the spin fluctuation on the triangular planes is quicker than those on the kagome lattice planes. The fact that the quick depolarization rate λ_q for $T < T_N$ is continuous with the λ_1 in the paramagnetic phase, implies a paramagnetic-like state for the Fe^{2+} spins on the triangular planes. Therefore, the models illustrated in Figs. 6(a) and 6(b) are favored.

IV. CONCLUSION

In summary, the rhombohedral structure $\text{Fe}_2(\text{OH})_3\text{Cl}$ [$\beta\text{-Fe}_2(\text{OH})_3\text{Cl}$] was synthesized in single phase and the crystal lattice was refined. The magnetic ions of Fe^{2+} in $\beta\text{-Fe}_2(\text{OH})_3\text{Cl}$ form a three-dimensional network of linked tetrahedra that can be viewed as alternatively stacked layers of kagome and triangular lattice planes along the (001) direction. Antiferromagnetic transition was observed at $T_N = 9.0$ K with a much larger Curie-Weiss temperature of θ_w of approximately -64 K, suggesting that $\text{Fe}_2(\text{OH})_3\text{Cl}$ is a geometrically frustrated magnet. Neutron-diffraction studies verified the transition into a long-range antiferromagnetic order below $T_N = 9.0$ K, for which possible magnetic structures are proposed. Of the four Fe^{2+} spins on a tetrahedron the one spin on the triangular lattice plane are disordered while the other three spins on the kagome lattice plane have frozen moments of less than 70% of the full Fe^{2+} moment. The most important results are the magnetically phase separation and the spin fluctuations coexisting with the long-range order. It is interesting that although the $\beta\text{-Fe}_2(\text{OH})_3\text{Cl}$ compound has a three-dimensional pyrochlore crystal structure, magnetically it can be viewed as an $S=2$ spin system with two-dimensional kagome correlations. The chemical bonding for the Fe^{2+} on the triangular lattice planes are different from those of the Fe^{2+} on the kagome lattice planes, which implies that selective substitution by nonmagnetic ions is possible. Such efforts are in progress to realize a chemically two-dimensional kagome lattice $\text{Fe}_3\text{Zn}(\text{OH})_6\text{Cl}_2$ and $\text{Fe}_3\text{Mg}(\text{OH})_6\text{Cl}_2$. It is worth noting that the transition occurs in a readily accessible range of temperatures, which is expected to facilitate future studies of spin correlation in geometrically frustrated systems.

ACKNOWLEDGMENTS

This work is supported by a Grant-in-Aid for Scientific Research (B) to X.G.Z. (Grant No. 19340100) from the Japan Society for the Promotion of Science (JSPS) and a Grant-in-Aid for Scientific Research on Priority Areas to X.G.Z. (Grant No. 20046012) from The Ministry of Education, Culture, Sports, Science and Technology (MEXT). We thank Kenji Ohoyama and Keiji Nemoto at Institute for Materials Research (IMR), Tohoku University for facilities during the neutron-diffraction experiment. We are grateful to Bassam Hitti, Donald Arseneau, and Syd Kreitzman at TRIUMF, Canada, for their continuing technical support.

*Author to whom correspondence should be addressed; zheng@cc.saga-u.ac.jp

- ¹For recent reviews see *Frustrated Spin Systems*, edited by H. T. Diep (World Scientific, Singapore, 2004); see also J. F. Sadoc and R. Mosseri, *Geometrical Frustration* (Cambridge University Press, Cambridge, England, 1999), reedited 2007.
- ²S. T. Bramwell and M. J. P. Gingras, *Science* **294**, 1495 (2001).
- ³M. J. Harris, S. T. Bramwell, D. F. McMorrow, T. Zeiske, and K. W. Godfrey, *Phys. Rev. Lett.* **79**, 2554 (1997); M. J. Harris, S. T. Bramwell, P. C. W. Holdsworth, and J. D. M. Champion, *ibid.* **81**, 4496 (1998); S. T. Bramwell and M. J. Harris, *J. Phys.: Condens. Matter* **10**, L215 (1998).
- ⁴A. P. Ramirez, A. Hayashi, R. J. Cava, R. Siddharthan, and B. S. Shastry, *Nature (London)* **399**, 333 (1999).
- ⁵J. S. Gardner, B. D. Gaulin, S.-H. Lee, C. Broholm, N. P. Raju, and J. E. Greedan, *Phys. Rev. Lett.* **83**, 211 (1999).
- ⁶J. S. Gardner, S. R. Dunsiger, B. D. Gaulin, M. J. P. Gingras, J. E. Greedan, R. F. Kiefl, M. D. Lumsden, W. A. MacFarlane, N. P. Raju, J. E. Sonier, I. Swainson, and Z. Tun, *Phys. Rev. Lett.* **82**, 1012 (1999).
- ⁷J. R. Stewart, J. S. Gardner, Y. Qiu, and G. Ehlers, *Phys. Rev. B* **78**, 132410 (2008).
- ⁸H. D. Zhou, C. R. Wiebe, J. A. Janik, L. Balicas, Y. J. Yo, Y. Qiu, J. R. D. Copley, and J. S. Gardner, *Phys. Rev. Lett.* **101**, 227204 (2008).
- ⁹I. Mirebeau, I. Goncharenko, H. Cao, and A. Forget, *Phys. Rev. B* **80**, 220407 (2009).
- ¹⁰X. G. Zheng and E. S. Otake, *Solid State Commun.* **130**, 107 (2004); X. G. Zheng and C. N. Xu, *ibid.* **131**, 509 (2004).
- ¹¹X. G. Zheng, T. Mori, K. Nishiyama, W. Higemoto, H. Yamada, K. Nishikubo, and C. N. Xu, *Phys. Rev. B* **71**, 174404 (2005); X. G. Zheng, T. Kawae, Y. Kashitani, C. S. Li, N. Tateiwa, K. Takeda, H. Yamada, C. N. Xu, and Y. Ren, *ibid.* **71**, 052409 (2005); X. G. Zheng, M. Hagihala, T. Kawae, and C. N. Xu, *ibid.* **77**, 024418 (2008).
- ¹²X. G. Zheng, H. Kubozono, K. Nishiyama, W. Higemoto, T. Kawae, A. Koda, and C. N. Xu, *Phys. Rev. Lett.* **95**, 057201 (2005); X. G. Zheng, T. Kawae, H. Yamada, K. Nishiyama, and C. N. Xu, *ibid.* **97**, 247204 (2006).
- ¹³M. Hagihala, X. G. Zheng, T. Toriyi, and T. Kawae, *J. Phys.: Condens. Matter* **19**, 145281 (2007).
- ¹⁴X.-G. Zheng, and K. Nishiyama, *Physica B* **374-375**, 156 (2006); X. G. Zheng, M. Hagihala, K. Nishiyama, and T. Kawae, *ibid.* **404**, 677 (2009); X. G. Zheng, T. Yamashita, M. Hagihala, and T. Kawae, *ibid.* **404**, 680 (2009); M. Fujihala, M. Hagihala, X.-G. Zheng, and T. Kawae, *ibid.* **404**, 674 (2009); M. Hagihala, X.-G. Zheng, and T. Kawae, *ibid.* **404**, 671 (2009); X. G. Zheng, M. Hagihala, K. Nishiyama, and T. Kawae, *J. Magn. Magn. Mater.* **310**, 1288 (2007); X. G. Zheng, M. Hagihala, M. Fujihala, and T. Kawae, *J. Phys.: Conf. Ser.* **145**, 012034 (2009).
- ¹⁵S.-H. Lee, H. Kikuchi, Y. Qiu, B. Lake, Q. Huang, K. Habicht, and K. Kiefer, *Nature Mater.* **6**, 853 (2007).
- ¹⁶A. S. Wills and J.-Y. Henry, *J. Phys.: Condens. Matter* **20**, 472206 (2008); *J. Phys.: Conf. Ser.* **145**, 012056 (2009).
- ¹⁷S. Maegawa, A. Oyamada, S. Sato, M. Nishiyama, T. Itou, and X. G. Zheng, *J. Phys.: Conf. Ser.* **145**, 012018 (2009).
- ¹⁸P. Mendels, F. Bert, M. A. de Vries, A. Olariu, A. Harrison, F. Duc, J. C. Trombe, J. S. Lord, A. Amato, and C. Baines, *Phys. Rev. Lett.* **98**, 077204 (2007).
- ¹⁹M. A. de Vries, J. R. Stewart, P. P. Deen, J. O. Piatek, G. J. Nilsen, H. M. Rønnow, and A. Harrison, *Phys. Rev. Lett.* **103**, 237201 (2009).
- ²⁰H. R. Oswald and W. Feitknecht, *Helv. Chim. Acta* **47**, 272 (1964).
- ²¹G. Springer, *Can. Mineral.* **27**, 311 (1989).
- ²²B. Saini-Eidukat, H. Kucha, and H. Keppler, *Am. Mineral.* **79**, 555 (1994).
- ²³E. Nishibori, M. Takata, K. Kato, M. Sakata, Y. Kubota, S. Aoyagi, Y. Kuroiwa, M. Yamakata, and N. Ikeda, *Nucl. Instrum. Methods Phys. Res. A* **467-468**, 1045 (2001).
- ²⁴F. Izumi and T. Ikeda, *Mater. Sci. Forum* **321-324**, 198 (2000).
- ²⁵K. Ohoyama, T. Kanouchi, K. Nemoto, M. Ohashi, T. Kajitani, and Y. Yamaguchi, *Jpn. J. Appl. Phys.* **37**, 3319 (1998).
- ²⁶A. S. Wills, *Phys. Rev. B* **63**, 064430 (2001).
- ²⁷P. Dalmas de Réotier, P. C. M. Gubbens, and A. Yaouanc, *J. Phys.: Condens. Matter* **16**, S4687 (2004).
- ²⁸J. Lago, T. Lancaster, S. J. Blundell, S. Bramwell, F. L. Pratt, M. Shirai, and C. Baines, *J. Phys.: Condens. Matter* **17**, 979 (2005).
- ²⁹P. Dalmas de Réotier, A. Yaouanc, L. Keller, A. Cervellino, B. Roessli, C. Baines, A. Forget, C. Vaju, P. C. M. Gubbens, A. Amato, and P. J. C. King, *Phys. Rev. Lett.* **96**, 127202 (2006).
- ³⁰F. Bert, P. Mendels, A. Olariu, N. Blanchard, G. Collin, A. Amato, C. Baines, and A. D. Hillier, *Phys. Rev. Lett.* **97**, 117203 (2006).
- ³¹R. S. Hayano, Y. J. Uemura, J. Imazato, N. Nishida, T. Yamazaki, and R. Kubo, *Phys. Rev. B* **20**, 850 (1979).